Enhancing the Gas Sensitivity of Surface Plasmon Resonance

with a Nanoporous Silica Matrix

Audrey Berrier[a], Peter Offermans[b], Ruud Cools[a], Bram van Megen[a], Wout Knoben[b], Gabriele Vecchi[a], Jaime Gómez Rivas[a], Mercedes Crego-Calama[b], Sywert Brongersma[b]

a) **Centre for Nanophotonics, FOM Institute AMOLF c/o Philips Research Laboratories, High Tech Campus 4, 5656 AE Eindhoven, The Netherlands**

b) **Holst Centre/imec-nl, High Tech Campus 31 , 5656 AE Eindhoven, The Netherlands**

ABSTRACT

The development of sensing schemes for the detection of health-threatening gases is an attractive subject for research towards novel integrated autonomous sensor systems. We report here on a novel way of sensing NO_2 by surface plasmon resonance (SPR) using a gas-sensitive layer composed of 5,10,15,20-Tetrakis(4-hydroxyphenyl)-21H,23H-porphine (2H-OHTPP) embedded in a nanoporous silica matrix on top of a gold thin film. The sensing mechanism is based on the modification of the SPR condition due to gas induced changes in the optical properties of the sensing layer. We demonstrate that the use of nanoporous silica as embedding matrix enhances the detection sensitivity compared to a polymer matrix with low porosity. The second important finding of this work is that the active layer thickness plays a significant role in the enhancement of the sensing response. The improvement is explained by the optimization of the overlap between the field of the surface plasmon polariton and the active dielectric layer.

Keywords: Nitrogen dioxide (NO_2), Gas Sensing, Surface Plasmon Resonance (SPR), Porphyrin , Porous matrix, Nanoporous silica.

1. Introduction

The detection of greenhouse gases (CO_2, NO_2, SO_2, CH_4) for outdoor monitoring and the control of health-threatening gases for indoor monitoring and building health assessment sets steadily growing demands for a simple, cost-effective and sensitive method for the detection of such gases in the ppb range. Many of the existing sensors are bulky or power hungry due to the need of a high operating temperature or large optical input power. For outdoor monitoring, remote sensing of greenhouse gases is possible with tunable mid infrared laser sources which require mW up to W of optical power [1]. For autonomous indoor monitoring systems, optical methods using light emitting diodes (LED) or halogen lamps with μW of optical power are, in this respect, more appropriate. Moreover, sensors relying on changes of the optical properties of an active sensing material operate at room temperature and remain immune to electrical interference effects.

In this work, we demonstrate surface plasmon resonance (SPR) based detection of NO_2 with a gas sensitive layer consisting of porphyrins [2] embedded in a nanoporous silica layer. We show that the use of porous silica as embedding matrix enhances the detection sensitivity compared to a polymer matrix with low porosity. We focus our attention towards ways of enhancing the interaction between the gas molecules, the porphyrins and the surface plasmon polariton field. It is not the purpose of this work to fully characterize a sensor, but rather to provide a method to improve the gas sensing mechanism based on surface plasmon resonances (SPRs).

The sensing mechanism at work here is based on SPRs, originating from the interaction of surface plasmon polaritons (SPPs) with their surrounding environment. SPPs are electromagnetic modes propagating at the interface between a dielectric and a metal, which is often gold owing to its good chemical stability. The SPP modes are extremely sensitive to changes in the permittivity of their dielectric environment [3]. SPR sensors have been investigated for many years in fields as varied as biotechnology [4], food monitoring [5] or health-care [6]. SPR sensing of NO_2 has been demonstrated with a limit of detection of 1 ppm [7,8]. Very recently a detection limit of 70 ppb was achieved using a silver layer in combination with lock-in detection [9]. However, most of the proposed systems use very thin layers of a few nanometers for the gas capture and do not fully exploit the decay of the intensity of the SPP from the surface, which is typically a few hundreds of nanometers. Here, we study a SPR-based system with ppb-level detection without the need for lock-in detection, therefore enabling easy integration for low power

devices. This system is based on the coupling of SPPs to porphyrins acting as sensing agents embedded in a nanoporous silica layer for structural purposes.

Porphyrins are highly conjugated macrocycles, which are known for their high chemical stability and possess a distinctive absorption spectrum in the visible range due to their electronic structures [10]. The capture of NO_2 by the porphyrin molecules gives rise to a characteristic absorption band around 680 nm [11], which modifies the permittivity and can be detected by a change in the SPR condition. The nanoporous silica layer enables control over the thickness of the active layer, allowing an easy gas diffusion through the porous structure of the layer and an optimized overlap of the SPP intensity with the active layer.

In the second section we present a description of the experimental details about sample fabrication, gas detection and optical measurements. In the third section we discuss the experimental results. We first present the influence of the porosity of the embedding matrix, before describing the response of the sensing layer as a function of the gas concentration. Finally we show that the sensing behavior can be improved if the active layer thickness is increased.

2. Experimental

2.1 Sample description

The sensitivity of the active layer to NO_2 depends on the ability of the gas molecules to reach the active adsorption sites on the porphyrin molecules. We propose that the gas reaches the active sites more easily if the porosity of the sensing layer is increased. To demonstrate this, we have investigated experimentally the response of four different types of sensing layers: *i*) a 10 nm thick layer consisting of only porphyrins, *ii*) a 65 nm thick layer consisting of embedded porphyrins in a nanoporous silica (NPS) matrix, *iii*) a 130 nm thick layer consisting of embedded porphyrins in an NPS matrix, and *iv*) a 65 nm thick layer consisting of porphyrins embedded in a polymer matrix (ethylcellulose, EC, low-porosity). Two more samples of NPS and EC without porphyrins were used as reference samples for sample *ii* and *iv*, respectively. The experiments performed with the considered samples are reported on Table 1. The ethylcellulose is a glassy polymer with a low fractional free volume (FFV) of 15% [12,13]. Even though it is possible that the FFV is modified due to the incorporation of porphyrins, we expect the pores to be small and unconnected. The increase of the FFV of EC by the use of a plasticizer has previously resulted in an

increase in the sensitivity of the layer [14]. The porosity of the NPS is 30% and the nanopores form an interconnected network fostering the diffusion of gas through the matrix.

2.2 Sample preparation

5,10,15,20-Tetrakis(4-hydroxyphenyl)-21H,23H-porphine (Sigma-Aldrich, Figure 1a) was dissolved in ethanol in a concentration of 5 g/l. For samples *ii* and *iii*, nanoporous silicon oxicarbide SiOC:H, which is a standard material for low k-dielectric materials in microelectronics [15], is used as embedding matrix. This nano-porous silica matrix (noted NPS) was mixed with the porphyrin solution (1:1) and further diluted (1:1) with ethanol. The NPS layer with embedded porphyrins was formed after spin-coating on SPR substrates. The SPR substrates consist of 50 nm thick gold layers on BK7 glass. The samples are spin coated at 3000 rpm for 30 s and baked at 200°C for 30 s. After this procedure the layer has a porosity of about 30% with a pore size of about 1 to 2 nm [12]. The NPS forms an interconnected network of nanopores providing an excellent pathway for gas diffusion. The absorbance spectrum of the active layer is characterized by a peak at 420 nm (Figure 1b) corresponding to the Soret band or B-band [10]. When the active layer is exposed to NO_2, the B-band red-shifts and an extra absorbance peak appears around 680 nm, the so-called Q-band. The development of the latter absorbance peak induces a permittivity change that can be sensitively detected following the evolution of the intensity of the SPR at the corresponding wavelength. Sample *iv* was prepared from an ethylcellulose solution in ethanol with the same concentration of porphyrins as with NPS solution. The sample was spincoated at 3000rpm, and baked at 175°C for 15 s. Sample types *ii*, *iii* and *iv* were obtained by spin coating from initial solutions prepared with identical porphyrin concentrations.

2.3 Gas setup and measurement procedure

Figure 2a represents a schematic diagram of the gas sensing setup used in this work. NO_2 is delivered into line 1 by a permeation tube emitting 2.3 μg/min when heated at 40°C. N_2 is used as carrier gas. The gas flow is directed towards an optical flow cell after further dilution in N_2 to a concentration in the range 290 to 6000 ppb (line 2). The flow is kept constant by introducing a mass flow controller (MFC) and a vacuum pump behind the flow cell. The minimum gas concentration was limited by the emission rate of the permeation tube and by the maximum flow allowed by the optical flow cell. This limit is 290 ppb in our setup. The gas concentration was calibrated by chemoluminescence measurements using an EcoPhysics chemoluminescence analyzer with a gas converter for catalytic conversion of NO_2 into NO. Prior to gas exposure, nitrogen gas was flushed over the sample in the flow cell for 20 min. This procedure removes

remaining traces of solvent, moisture and oxygen from the atmosphere of the flow cell before sensing. After gas exposure, recovery of the active layer is performed within a few minutes by gentle heating (75°C) under N$_2$ flow in order to desorb the trapped NO$_2$ molecules.

2.4 Optical methods

To characterize the behavior of the sensing layer, we have carried out attenuated total internal reflection (ATR) measurements in the Kretschmann configuration [16] as well as specular reflectance measurements.

The ATR method is used to detect changes in the SPR condition upon gas exposure. In this configuration (Figure 2b), the sample is fixed on a half-cylindrical lens acting as a prism by a droplet of refractive index matching liquid (n=1.51). A rotational stage allows the independent setting of the angle of incidence and of the detection angle. A halogen lamp is used as the light source and a fiber coupled spectrometer is used as a detector. The polarization of the incident light is controlled with a polarizer.

The variation of the permittivity of the sensing layer due to the reaction with the gas modifies the SPR condition, which is monitored by a measurement of the spectrally and angularly resolved ATR reflectance (SARR). The SARR is a measurement of the coupling of the incident light to SPPs. This coupling takes place when the parallel component of the wave vector of the incident radiation in the prism with respect to the interface,

$$k_{//} = \frac{2\pi}{\lambda} n_p \sin\theta \qquad , \tag{1}$$

is equal to the wavevector of the SPP

$$k_{SPP} \approx \frac{2\pi}{\lambda} \text{Re}\left(\sqrt{\frac{\varepsilon_{metal}\varepsilon_{layer}}{\varepsilon_{metal}+\varepsilon_{layer}}}\right), \tag{2}$$

where λ is the wavelength in vacuum, θ is the angle of incidence, n_p is the refractive index of the prism, ε_{metal} is the complex permittivity of the gold layer and ε_{layer} is the complex permittivity of the active layer. We note here that due to the finite thickness of the active layer the mode will be perturbed with respect to the mode existing at the interface of an infinitely thick active layer.

Specular reflectance measurements were also carried out on the samples for real time characterization of the absorbance of the active layer. For these measurements, the incident angle is chosen to be 20°.

3. <u>Results and discussions</u>

In this section we are reporting our results on the influence of the porosity of the active layer, on the gas concentration, and on the thickness of the active layer. A model based on the transfer matrix method is used to fit the experimental data and study the influence of the field overlap with the active layer on the sensitivity of detection.

3.1 Influence of the porosity and thickness of the active layer

The influence of the porosity and thickness of the active layer was investigated by performing ATR and reflectance measurements. Table 1 summarizes the behavior of the investigated samples. ATR measurements performed on sample *i*, i.e., the 10 nm thick layer of porphyrins, result in very weak, almost undetectable changes of the SPR signal (experiment A in table 1). The reflectance change after exposure to a high gas concentration of 6 ppm is only 1.5%. Several effects may be at play explaining this lack of sensitivity: porphyrin molecules are often prone to aggregation into clusters which renders them less sensitive to binding with gas molecules [17]; furthermore, the overlap of the evanescent field of the SPP with the active layer is relatively small. SPPs on gold decay from the surface with a characteristic decay length of 190 nm, at 680 nm, for a gold/air interface. Therefore, the use of an embedding matrix is expected to both reduce the probability of aggregation of the porphyrins and to increase the interaction of the active layer with the evanescent field of the surface plasmon. Indeed, when using NPS as embedding matrix with a thickness of 65 nm (sample *ii*), ΔR obtained by ATR for a gas concentration of 700 ppb is 17%. We also note that the ATR reflectance change is about twice as large as that of the specular reflectance (experiments B, C in table 1). Interestingly, doubling the thickness of the layer increases ΔR by almost a factor of five (experiments D, F in table 1). In section 3.3, we will see that the enhanced sensitivity of ATR can be explained by the increased overlap of the SPP and the active layer. The use of a porous matrix is there essential as it allows the enhanced diffusion of gas into the matrix. This is confirmed by the fact that when using an EC polymer as embedding matrix of identical thickness we find that the specular reflectance is reduced by a factor of four (experiments C, G in table 1). Thus, by the use of a thick, porous embedding matrix the sensitivity of the SPR sensing can be strongly enhanced, enabling the detection of NO_2 concentrations in the ppb range as demonstrated in the next section.

3.2 Influence of the gas concentration

Figure 3 compares the spectrally and angularly resolved ATR reflectance (SARR) as a function of gas concentration for a sample with a 65 nm thick layer of NPS with embedded porphyrin molecules. The reflectance dip (Figure 3a) is due to the coupling of the incident light to SPPs. Its shape is governed by dispersion and loss of the SPP mode. The exposure of the sample to NO_2 modifies the dispersion relation of the SPP due to the change in the permittivity of the active layer. Figure 3b shows the change in reflectance after exposure to an NO_2 concentration of 4600 ppb. The reflectance dip evolves into two separate branches, which is due to the enhanced absorption due to the interaction of NO_2 with the porphyrin layer. This splitting into two new polaritonic branches can be explained by a mode coupling between the excitonic states of the porphyrins and the SPP modes. The analysis of the physics of the mode coupling is out of the scope of the present work and will be the object of a separate article. The splitting depends on the change in permittivity of the sensing layer. When exposing the sample to a much lower concentration C=350 ppb the splitting is strongly reduced (Figure 3c). However, the presence of NO_2 in the layer is still detectable: as shown in Figure 3d, the reflectance at the wavelength of 680 nm increases by about 20% and shifts with an angle of 0.6^{o} for an exposure to a concentration as low as 290 ppb, indicating that even lower concentrations may be detected. Note that the concentration of 290 ppb is the lowest we can flow controllably in our setup.

SPR-based sensing can be performed by detection of the shift in resonance angle or wavelength, and by changes in reflectance. The reflectance around 680 nm, which originates from the change in the imaginary part of the refractive index (extinction coefficient of the active layer) is shown as function of gas concentration in Figure 4a. We observe that the reflectance minimum increases with NO_2 concentration in a non-linear fashion. Two regimes can be defined: between 0 and 1000 ppb the reflectance increases steeply with concentration at a rate of about $3x10^{-4}$/ppb, whereas after 1000 ppb the increase in reflectance saturates. Alternatively, we can also monitor the shift in wavelength of the reflectance minimum at a fixed angle. The splitting of the resonance curve results in a contribution to the wavelength shift to both longer and shorter wavelengths. The monitoring of the wavelength shift towards longer wavelengths, as shown on Figure 4b, gives a resolution of $8x10^{-2}$ nm/ppb in the low concentration regime and of $5x10^{-3}$ nm/ppb in the high concentration regime. The response time of the system is of the order of minutes, which is short enough for pollution level monitoring applications.

3.3 Influence of the SPP field overlap with the sensing layer

The electric field of the SPP at the interface between the metallic and an infinitely thick active layer, for which *n*=1.42, is evanescently decaying within the dielectric layer with a characteristic decay length of about 150 nm. Even though one notes that the field decay will be modified by the finite thickness of the active layer, it is possible to enhance the interaction between the active layer and the SPP field by increasing the active layer thickness. We experimentally determine the influence of the layer thickness by comparing the SARR plots of the sample with thickness of 65 nm (sample *ii*) with the sample with a thickness of 130 nm (sample *iii)*, as shown in Figure 5a and 5b, respectively (see also Table 1)**.** Both investigated samples were exposed to a NO_2 concentration of 350 ppb. As expected, the SPR shifts towards larger angles when the thickness of the active layer increases. In contrast to the case with the 65nm layer, for the 130 nm thick layer the splitting of the resonance is clearly visible although the same gas concentration was used. Both the change in reflectance and the splitting of the resonance $\Delta\lambda$ increase when the active layer is thicker, as indicated by the line cuts displayed in Figure 5c, which represents an angular cut at the middle of the curve splitting, as indicated by the dashed line seen on Figure 5a and b. Thus, the experimental results confirm that the sensitivity increases with a larger thickness of the active layer. The separation between the two reflectance dips at a given angle (which is noted $\Delta\lambda$ in the following) is defined on Figure 5c. The magnitude of the splitting $\Delta\lambda$ is measured at the angle where both reflectance dips reach down to the same value.

To further investigate the dependence of the sensing behavior on the thickness of the active layer, we model the reflectance of the layered system using the transfer matrix method, incorporating the complex permittivity of each individual layer. The change in permittivity of the active layer around 680 nm due to gas interaction in the active layer is calculated using a Lorentzian model following the equation:

$$\varepsilon(\nu) = \varepsilon_b(\nu) + \frac{F\nu_0^2}{\nu_0^2 - \nu^2 - i\gamma\nu} \qquad (3)$$

where ε_b is the complex permittivity of the background, ν_0 is the frequency of the absorption line , γ is the damping rate of the transition and ν the frequency. *F* is a parameter proportional to the oscillator strength of the active layer, which depends on the number of NO_2-porphyrin interaction sites and, by extension, on the gas concentration. The damping rate γ and the value of *F* are obtained from the fit of the experimental data for a layer thickness of 130 nm and gas concentration of 350 ppb. The *F* factor is subsequently varied proportionally to the gas concentration, whereas γ is, for sake of simplicity, kept constant (γ=3.2 10^{13} rad.s^{-1}). Figure 5d presents the result of the modeling for the 130nm thick active layer with *F*=40.10^{-4}. The

agreement with the experimental SARR plot is very good, indicating the validity of the model. Further, calculations for various layer thicknesses and gas concentrations are performed in order to gain further insight into the sensing behavior and optimize the sensing layer.

The plots in Figure 6 are obtained point by point: for each thickness and gas concentration we calculate the SARR plot from which $\Delta\lambda$ is directly measured from the angular cross section with reflectance dips reaching down to the same value. Figure 6 displays the dependence of $\Delta\lambda$ as a function of the layer thickness for three different F parameters. It also compares the calculations with the experiments. The experimental points, corresponding to data from figure 3b and 5a-b, are indicated by the black diamonds and the hexagon. From the model we find that $\Delta\lambda$ increases with the layer thickness, in agreement with experimental observation. $\Delta\lambda$ starts to level off as the thickness of the active layer increases further than about 300 nm.

This dependence is explained by the overlap between the SPP field profile and the active layer. $\Delta\lambda$ increases with increasing overlap of the SPP field profile with the active layer and saturates when the SPP field profile decays fully within the active layer. We may expect that the thickness for optimum sensitivity will depend on the porosity of the embedding matrix of the active layer as it is expected to be a trade-off between increased gas diffusion times and increased field overlap with the active layer. We note that the diffusion of NO_2 through the active layer and its interaction with the porphyrin molecules may have a direct impact on the spatial dependence of the imaginary part of the refractive index $k=k(z,\lambda)$, which is not taken into account in the present modeling. The modeling of the diffusion of NO_2 molecules through the matrix, their adsorption and reaction with the porphyrin molecules is out of the scope of the present work. Here we are approximating $k(z,\lambda)= k(\lambda)$ for $z<h$, and $k(z,\lambda)= 0$ for $z>h$, with h the thickness of the active layer. Our simplified model shows that the sensitivity of an SPR based sensing system can be enhanced if the active layer thickness is optimized. The comparison of the modeled curve with the experimental points suggests that the optimum layer thickness is larger than 130 nm.

4. Conclusions

Optical sensing of nitrogen dioxide has been demonstrated using surface plasmon polaritons at the interface between a gold layer and a porous silica layer containing porphyrins. The penetration of NO_2 molecules into the sensitive layer induces a characteristic absorption peak that modifies the dispersion curve of the SPP. Detection of NO_2 gas in the 100s ppb range was experimentally achieved, with potential for sensitivity down to few tens of ppb. It is demonstrated that the sensing system can be improved by: (i)

increasing the porosity of the porphyrin embedding matrix; and (ii) by increasing the active layer thickness maximizing the field overlap with the gas reactive regions. Although the sensing mechanism was characterized for NO_2 detection, the sensitivity enhancement strategy presented here is applicable to other SPP-based gas sensors, with an adaptation of the sensing molecule to the gas to be detected.

References

[1] A. Berrou, M. Raybaut, A. Godard, M. Lefebvre, High resolution photoacoustic and direct absorption spectroscopy of main green house gases by the use of a pulse entangled cavity doubly resonant OPO, Appl. Phys. B 98, (2010) 217-230.

 [2] D. Dolphin, The Porphyrins, Academic Press, New York (1978).

 [3] H. Raether , Surface plasmons on smooth and rough surfaces and on gratings , Springer tracts in Modern Physics, Vol. 111, (1988) Springer-Verlag.

[4] T. Wangkam, T. Srikhirin, P. Wanachantararak, V. Baxi, B. Sutapun and R. Amarit , Investigation of enzyme reaction by surface plasmon resonance (SPR) technique , Sens. Actuators B 139, (2009) 274-279.

[5] J. Ladd, A. D. Taylor, J. Homola, S. Jiang, Detection of botulinum neurotoxins in buffer and honey using a surface plasmon resonance (SPR) sensor, Sens. Actuators B 130, (2008) 129-134.

[6] M. J. Linman, K. Sugerman, Q. Cheng, Detection of low levels of Escherichia coli in fresh spinach by surface plasmon resonance spectroscopy with a TMB-based enzymatic signal enhancement method, Sens. Actuators B 145, (2010) 613-619.

[7] G.J. Aswell and M.P.S. Roberts, Highly selective surface plasmon resonance sensor for NO_2 , Elec. Lett. 32, (1996) 2089.

[8] J. D. Wright, A. Cado, S. J. Peacock, V. Rivalle and A. M. Smith, Effects of nitrogen dioxide on surface plasmon resonance of substituted phtalocyanine films, Sens. Actuators B 29 (1995) 108-114.

[9] A. B. El-Basaty, T.A. El-Brolossy, S.Abdalla, S. Negm, R.A.Abdella and H. Tallat , Surface plasmon sensor for NO_2 gas , Surf. Interface Anal. 40, (2008) 1623-1626.

[10] M. Gouterman , Spectra of porphyrins , J. Mol. Spectrosc. 6, (1961) 138.

[11] A. J. Mc Naughton, T. H. Richardson, W. Barford, A. Dunbar, J. Hutchinson, C.A.Hunter , Characterisation of the reaction of free-base porphyrins to nitrogen dioxide , Colloid. Surf. A 284, (2006) 345-349.

[12] . A. Thran, G. Kroll, F. Faupel, Correlation between fractional free volume and diffusivity of gas molecules in glassy polymers, J. Polym. Sci. B 37, (1999) 3344-3358.

[13] J. Qiu, J.-M. Zheng, K.-V. Peinemann, Gas transport properties of Poly(trimethylsilylpropyne)and Ethylcellulose filled with different molecular weight trimethylsilylsaccharides: Impact on fractional free volume and chain mobility , Macromolecules 40, (2007) 3213-3222.

[14] Y. Itagaki, K. Deki, S.-I. Nakashima, Y. Sadaoka, Toxic gas detection using porphyrin dispersed polymer composites, Sens. Actuators B 108 (2005) 393-397.

[15] K. Maex, M. R. Baklanov, D. Shamiryan, F. Lacopi, S. H. Brongersma, and Z. S. Yanovitskaya, Low dielectric constant materials for microelectronics , J. Appl. Phys. 93, (2003) 8793.

[16] E. Kretschmann , The determination of the optical constants of metals by excitation of surface plasmons , Z. Phys. 241, (1971) 313-324.

[17] R.F. Pasternack, P.J. Collings, Resonance light-scattering – A new technique for studying chromophore aggregation , Science 269, (1995) 935-939.

[18] K.Kurihara, K.Suzuki , Theoretical understanding of an absorption based surface plasmon resonance sensor based on Kretschmann's theory , Anal. Chem. 74, (2002) 696-701.

Table 1: Comparison of the reflectance change as a function of the experimental conditions of the sample thickness, matrix (NPS: nanoporous silica, EC ethylcellulose), presence of porphyrin molecules, gas concentration and optical method (Refl: reflectance, ATR: attenuated total reflectance, ΔR: variation of reflectance at a wavelength of 680 nm and at the angle corresponding to the minimum of reflectance of the unexposed sample).

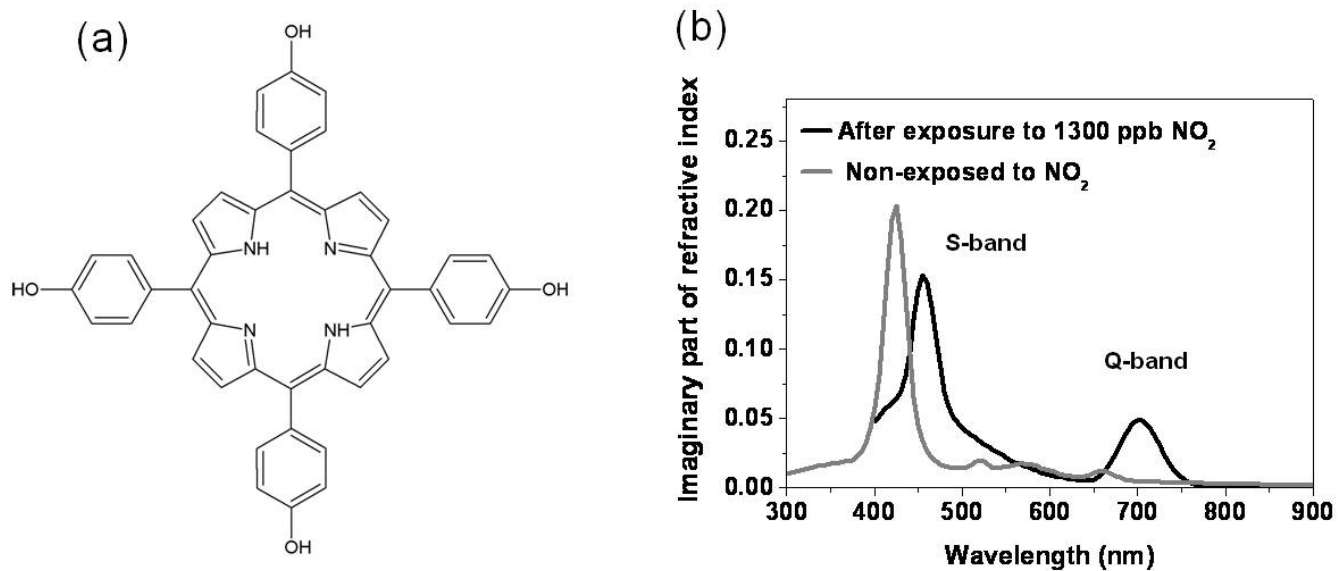| Experiment	Sample type	Layer thickness h (nm)	Matrix	Porphyrins	$[NO_2]$ (ppb)	Optical method	ΔR (%)
A	*i*	10	None	Yes	6000	ATR	1.5
B	*ii*	65	NPS	Yes	700	ATR	17
C	*ii*	65	NPS	Yes	700	Refl	8
D	*ii*	65	NPS	Yes	350	ATR	3
E	*ii*-ref	65	NPS	No	4600	ATR	0
F	*iii*	130	NPS	Yes	350	ATR	14
G	*iv*	65	EC	Yes	700	Refl	2
H	*iv*-ref	65	EC	No	700	Refl	0

Fig. 1. (a) 5,10,15,20-Tetrakis(4-hydroxyphenyl)-21*H,23H*-porphine (abbreviated as 2H-OHTPP) ; (b) Imaginary part of the refractive index (i.e., the extinction coefficient *k*) of the porphyrin layer embedded in a nanoporous silica matrix as obtained by ellipsometry, before and after exposure to the NO_2 gas.
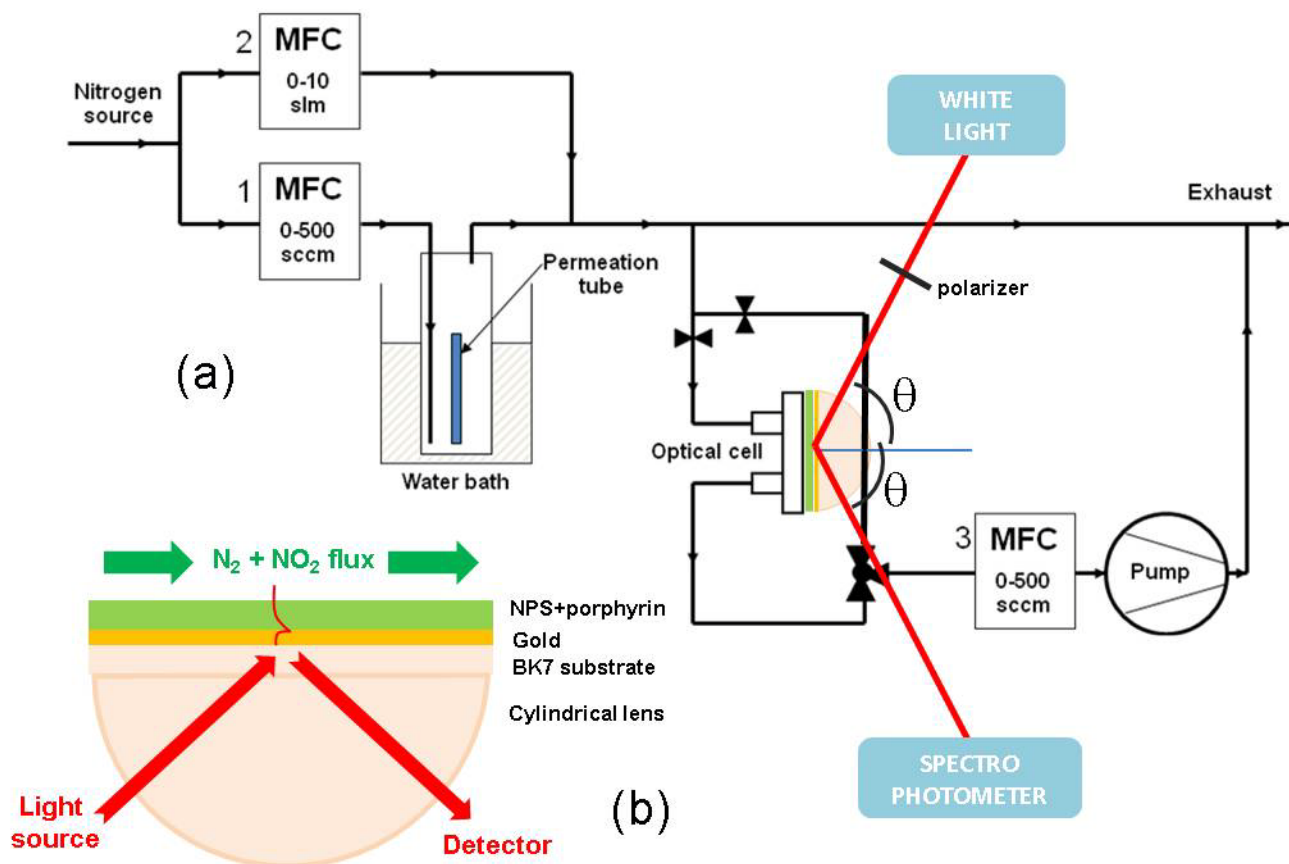
Fig. 2. (color online) Schematic diagram of the experimental set up for gas sensing (a) diagram indicating the gas flow system as well as the optical flow cell and optical path. 1 indicates the main flow path, 2 is the purge path and 3 is the exhaust path (MFC: mass flow controller, sccm: standard cubic centimeter per minute, slm: standard liter per minute); (b) schematic drawing zoomed around the sample. The electric field profile of the surface plasmon polariton at the interface between the gold layer and the active layer is schematically represented by the red curve.

Fig. 3. (color online) ATR reflectance of a sample with active layer thickness t=65 nm as a function of the wavelength and of the angle of incidence of the light with respect to the normal to the layer. The dip in reflectance (blue area) indicates the coupling to the surface plasmon at the gold-porphyrin layer interface. a) before NO_2 exposure; b) after exposure to 4.6 ppm NO_2; c) after exposure to 350 ppb NO_2; d) Reflectance at 680 nm before and after exposure to NO_2 with a concentration of 290 ppb.
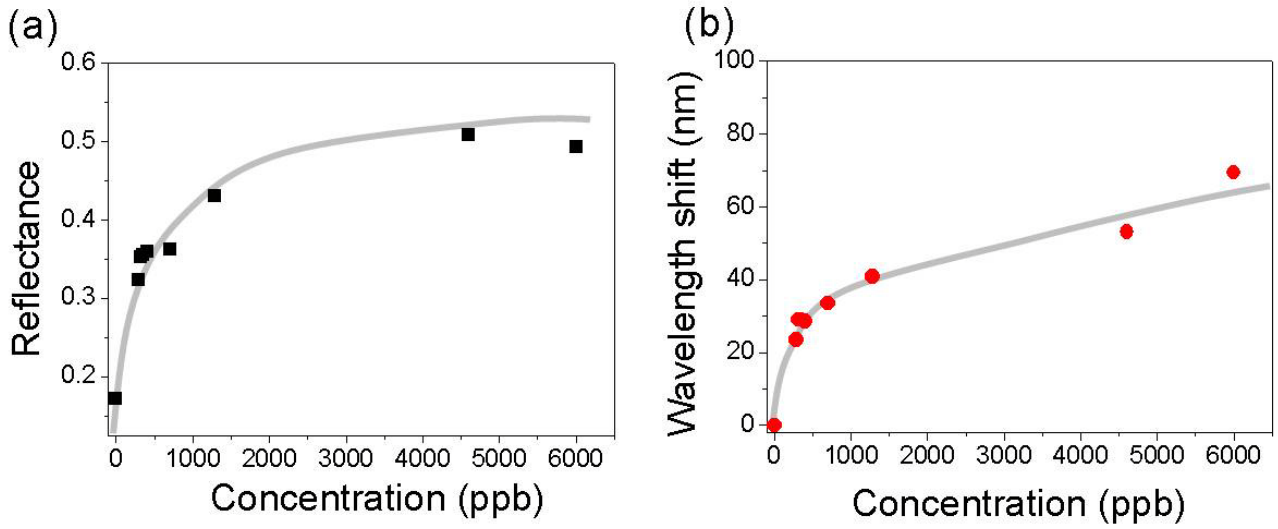
Fig. 4. (a) ATR reflectance at 680 nm as a function of the NO_2 concentration at equilibrium. (b) Resonance wavelength as a function of NO_2 concentration at an angle of 53.5°. The grey lines are guides to the eye.
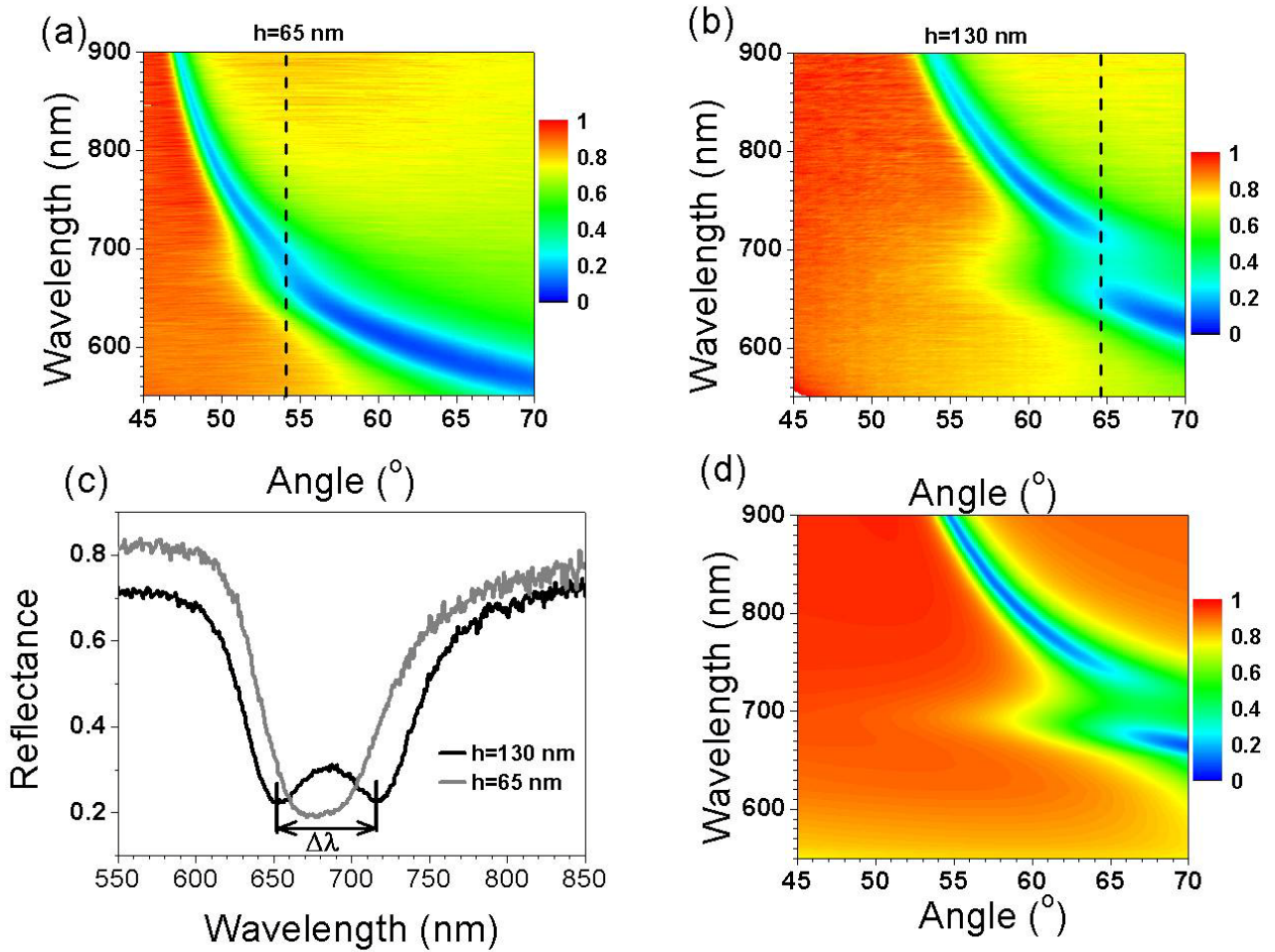
Fig. 5. (color online) (a) Experimental spectrally and angularly resolved ATR reflectance (SARR) plot for an active layer thickness h=65 nm after exposure to 350 ppb NO_2 ; (b) Experimental SARR plot for an active layer thickness h=130 nm after exposure to 350 ppb NO_2; (c) Angular cuts of the SARR plots for the two thicknesses (at the position of the respective dashed lines in a) and b)); (d) Calculated SARR plot for an active layer thickness of 130 nm with F=40.10^{-4}.
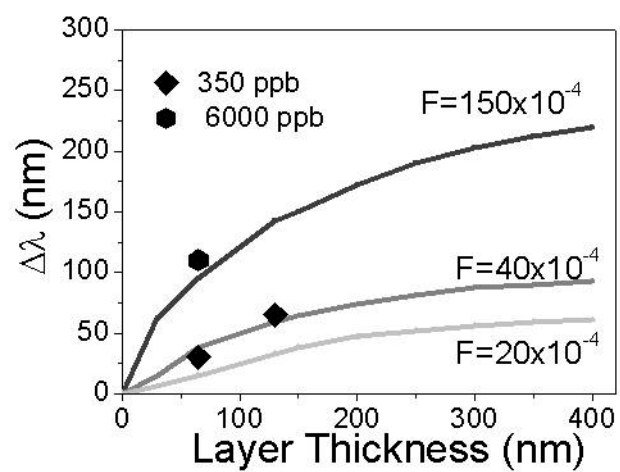
Fig. 6. Evolution of the calculated $\Delta\lambda$ as a function of the active layer thickness for three different values of the oscillator coefficient F, the black dots correspond to experimental points. The diamonds correspond to an exposure to 350 ppb of NO_2 and a layer thickness of 65 and 130 nm. The black hexagon corresponds to an exposure to 6000 ppb of NO_2.